CB03 - A New Prototype for Acousto-Ultrasound Analysis of Carbon Anodes

Daniel Rodrigues[1], Carl Duchesne[2] and Donald Picard[3]
1. Ph.D. Candidate, Aluminum Research Centre – REGAL, Département de génie chimique,
2. Professor, Aluminum Research Centre – REGAL, Département de génie chimique,
3. Research Assistant, Aluminum Research Centre – REGAL, Département de génie civil,
Université Laval, Québec, Canada
Corresponding author: carl.duchesne@gch.ulaval.ca

Abstract

A new acousto-ultrasonic (AU) system was developed for non-destructive assessment of damages within pre-baked carbon anodes manufactured for the Hall-Héroult process. It improves over the technique used in past research made in the group by collecting information in a more representative manner, and receiving the same signal simultaneously in multiple positions. Therefore, AU measurements are more robust and redundant, decreasing the probability for a false evaluation. Moreover, the system can analyze full-scale anodes rapidly and in a more standardized way, reducing variation caused by human manipulation of probes and increasing the system's capacity. The AU system described in this paper is mounted on a forklift. A proof-of-concept is presented where the system is used to collect measurements on a small population of anodes in all stages of fabrication (green, baked, slotted, and rodded). The AU response of the anodes is analyzed with the aid of latent variable modelling. Results are compared between anode types and confronted with expected properties of each type of anode. Additionally, an assessment of repeatability of the results is also shown.

Keywords: Pre-baked carbon anodes, non-destructive testing, acousto-ultrasonics, latent variable modelling, repeatability.

1. Introduction

For every kg of aluminum produced by the Hall-Héroult process (H-H), 4 kg of bauxite, 0.4-0.5 kg of carbon, 13-15kWh of energy and some other additives are consumed [1]. Approximately 1% of all the greenhouse gases (GHG) emitted by metal production in the world come either as direct emissions or embodied emissions from aluminum production [2], and one of the key components in this process is the pre-baked carbon anode, the carbon source for the H-H process. Anode quality can affect smelter performance to the point of increasing GHG emission by more than 60% in addition to a 100$/t Al cost increase [3]. Quality parameters for anodes are not a new subject, nor a static one. What is considered good has changed with time both in terms of anode properties and their ranges [4–8]. An important issue throughout the industry is to manufacture consistent quality anodes [9].

A major part of the anode's mass is calcined petroleum coke (CPC), ranging from 63 %-70 % [10], which has been subject to a major quality change in the last two decades. The concentration of contaminants has steadily increased while its properties also are becoming more variable as a consequence of the new oil market dynamics [11–13]. Back several years when CPC supply was more stable, standard chemical and physical characterizations of anode properties in the lab based on core samples were more than sufficient to assess anode quality. However, in actual conditions, the typical 4-6 weeks delay before lab results are available does not allow for timely monitoring of anode quality. Moreover, core sampling rates are typically under 2% of the weekly anode production. The core sample themselves consists of only approximately 0.3% of the volume of a 1-ton anode, from which a set of 15 properties are measured and assumed representative of the

anode volume. This procedure for assessing anode quality has been criticized as excessively complex [14] and potentially unnecessary. Additionally, because of the positioning of such samples and their small volumetric fraction of the whole anode body, physical defects that exist in different internal anode sections, such as cracks, are not necessarily detected, even though those are detrimental to the anode quality.

Non-destructive testing (NDT) could be a solution to these problems in the modern anode quality control system. Since the 1970s, researchers have been aware of how positive would be the capacity of analyzing full-sized anodes without destroying them and having a smaller delay to obtain the results necessary for making a decision. It would significantly increase the fraction of analyzed anodes and deliver a much faster response time to smelter operations, increasing the potential of a more profitable aluminum smelter. Multiple sensing principles can be used to create an applicable NDT.

Electrical resistivity is the oldest technology when referring to NDT applied to carbon anodes. In the 1970s an instrument for measuring baked anode resistivity was developed [15, 16]. It was made with an array of 40 current and 9 voltage probes on the bottom of the anode to measure both current and voltage simultaneously while mimicking the current pathway during full-scale operation. Although the method measures a repetitive average value, it is not capable of sizing, positioning or differentiating existing defects on an anode precisely because it only gives this average value that represents the anode as a whole.

Focused on the idea of reproducing the current distribution of an anode in service, the MIREA device was developed [17–20]. It has since then been extensively tested in more than 10 000 baked anodes. Instead of probes applied on the bottom of the anode, a current is passed through from the stub holes to a carpet at the anode's bottom while voltage drop is measured at different heights on the anode sides. Although it has not shown the capacity of differentiating the types of defects, one could argue that it is roughly capable of detecting its position through a higher resistivity measurement in a specific zone of the anode volume. Overall, the method shows that it can measure the electrical resistivity of an anode with a good representativity of the whole anode body, but differentiating the types of defects is not claimed.

Aforementioned resistivity techniques were all focused on baked anodes, which is not the case with the SERMA device [21–28]. Green anodes cannot suffer high currents passing, for those may affect the distribution of pitch due to heating. For that, the system was adapted to run at low currents. It consists in pairs of metal plates to which a matrix of voltage and current probes are assembled to measure the electrical current distribution through the anode volume. The pairs of plates are contacted on opposite sides of the anode and a controlled current is passed through. This is done both from top to bottom and from the anodes' sides, and the combination of both information is used to identify the position where defects may exist. However, this method may cause ambiguities on the positioning of those defects if multiple exist, and because the electric current passes through the least resistance pathway, one cannot be sure of the exact path where the currents have passed, complicating the positioning even more.

Another device focused on the green anode [29] is a combination of multiple four-points probes (4PP) [30]. This device combines 4 probes located in different positions on the anode's long side and 1 on the shorter side to measure the specific electrical resistivity. The data extracted from more than 120 000 anodes using this device was used as the input to build a system to predict baked anode sticking issues when unloading from baking furnaces [31]. One of the main issues with the system is contacting. This is true of most electrical resistivity-based NDTs, and it was one of the motivators to the development of contactless technologies.
Using metals coils, Haldemann & Fawzi [32, 33] designed an equipment that would generate eddy currents inside the anode when using an alternating magnetic field. As a consequence, the

coil used for that field would suffer an impedance that is consequence of the generated eddies, and would be correlated with the anode. An evolution of the concept [34] was designed later that used three axis-aligned coils: one for the emission of the magnetic field, and the other two equally separated, with the first one in the middle. The two coils are connected and spun in different directions guaranteeing that if there is no interfering body between the equipment, no current is to be induced in the two receiving coils. When an anode passes through the coils, it interferes in the magnetic fields inside each of the coils by changing the magnetic field permeability of the space in which the field exists, causing a specific current signal in the coils. Although, truly contactless the previously discussed methods raise concerns as to whether the currents can penetrate the anode's surface and if they would be feasible in an industrial setting.

Acoustic properties were explored first in 1981 [35] (and possibly earlier but not publicly documented) through the measurement of the speed of a 150 kHz wave by measuring the flight time it takes to propagate through the anode body along its length. A significant drop in that speed compared to the rest of the body suggests the existence of a defect in the pathway of the slower measurement. This concept was proven by sawing 90 anodes and confirming the existence of internal damage in the regions with abnormal measurements. An evolution of that technique is the one developed by Ben Boubaker *et al.* [36–38], which uses a 100-300 kHz modulated ultrasound wave in multiple specified positions to evaluate anode integrity. The method is capable of roughly positioning defects and differentiating them between cracks and abnormal porosity. That is the first technique that shows significant capacity to differentiate defects on full-scale baked anodes, while still being capable of positioning.

Acousto-Ultrasound (AU) analysis, as it was named, was only tested on a small number of full-scale anodes [36–38]. To further validate the proposed method, application to a more comprehensive set of anodes is required. Thus, a new procedure that is less manual than what was executed in this previous work, that is faster, and implementable in an industrial environment is required. This work targets precisely the evaluation of a prototype equipment for such an analysis.

2. Methodology

Twelve full-scale anodes were used to evaluate the new prototype: 3 green, 3 baked, 3 sawed to create slots, and 3 rodded anodes. For each anode tested using the prototype, the AU measurements were repeated fives at each position on the blocks by removing the sensors, putting them back in contact with the anode, and collecting the AU signals again. This procedure was used to evaluate how much variability originates from the equipment itself.

The signals acquired are then decomposed into different frequency bands using the Continuous Wavelet Transforms (CWT). A set of features are subsequently extracted from each band. These features representing the unique AU signature of the anodes are finally analyzed using Principal Component Analysis (PCA) to cluster the carbon blocks and reveal their differences. The PCA model results are used to evaluate:

- AU measurement repeatability
- Discrimination capacity based on production stage (i.e., green, baked, sawed and rodded anodes)
- Discrimination capacity of individual anodes

The following subsections describe the new equipment, and how AU data are acquired, processed and analyzed.

2.1 Acousto-Ultrasound Equipment

A drawing of the prototype is shown in Figure 1. A global view of the equipment is presented in Figure 1b) and the sensor arrangement is shown in Figure 1a). The system is equipped with eight R6-α general purpose 60 kHz resonant acoustic sensors are used for the Acousto-Ultrasound (AU) measurements on a 1 MHz frequency. Seven sensors (i.e., receivers) are positioned on an aluminum structure fit on a manual forklift to be placed under the anode block. The sensor arrangement (Figure 1a)) lets the two lateral sensors (2 and 8) move freely along the blue and red supports directions so that they can better explore the extremities of the anodes. Sensors 3 to 7 are fixed on the middle of the anode, where most cracks are typically located. Sensor 1 (not shown in the Figure 1) is the emitter for the modulated ultrasonic signal used to excite the anode blocks at different positions. Sensors 2-8 are connected to an amplifier which sends the captured signal to the data acquisition system.

The wheels distance to the box is adjustable to guarantee the centering of the middle row of sensors. This ensures that when the wheels are in contact with the anode, the sensors are positioned in the desired locations. Anodes are placed over two supports, leaving very little space for the forklift to pass under the blocks. This helps positioning of the system in a repeatable manner.

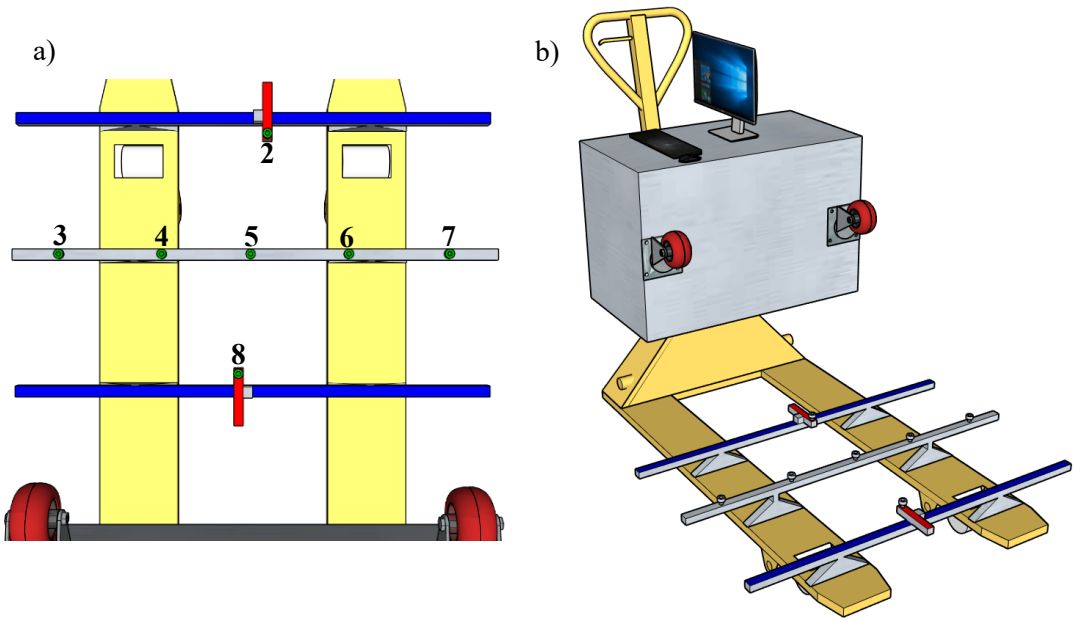

Figure 1. a) AU sensor arrangement (receivers). b) global view of the equipment.

The signal is emitted from sensor 1 positioned on top of the anodes, passes through the carbon block and is received by all sensors as depicted in Figure 2Figure . It results in a more robust measurement, capturing the waves emitted by sensor 1 propagating through the same region but following different paths.

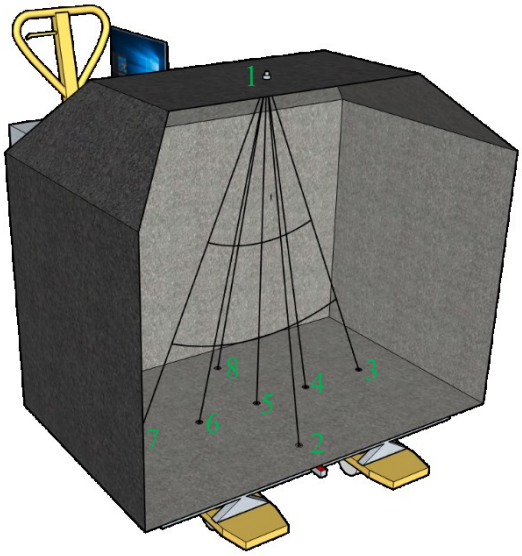

Figure 2. Signal pathways for an AU analysis from a specific point in the anode's surface with sensor numbers.

The procedure is repeated 21 times, by moving the emitter (sensor 1) to the different positions shown in Figure 3. Sensors 2 and 8 are moved together with the emitter to ensure they are aligned (i.e., when moving from emitter position 3 to 4, sensors 2 and 8 are moved to be under the line that goes from position 4 to 6).

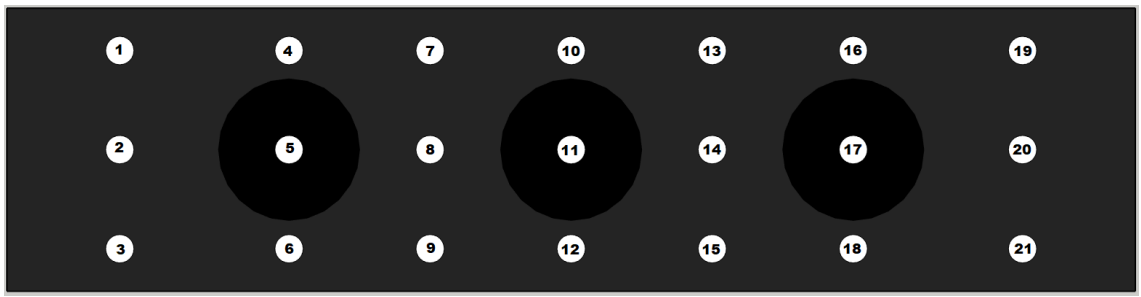

Figure 3. Positioning of the AU excitation signal emitter (top view of the anode).

The signal emitted by sensor 1 is modulated as presented in Figure 4. This modulated signal was tailor-made to be decomposed using the continuous wavelet transform using the "Bump" wavelet. The objective is to obtain as many different frequencies as possible in the excitation signal while eliminating overlapping between bands. This way any correlation found between different frequencies would not be an artifact of the transformation. Such requirement for the frequencies is based on the observation that each frequency interacts differently with the anode's internal structure [38].

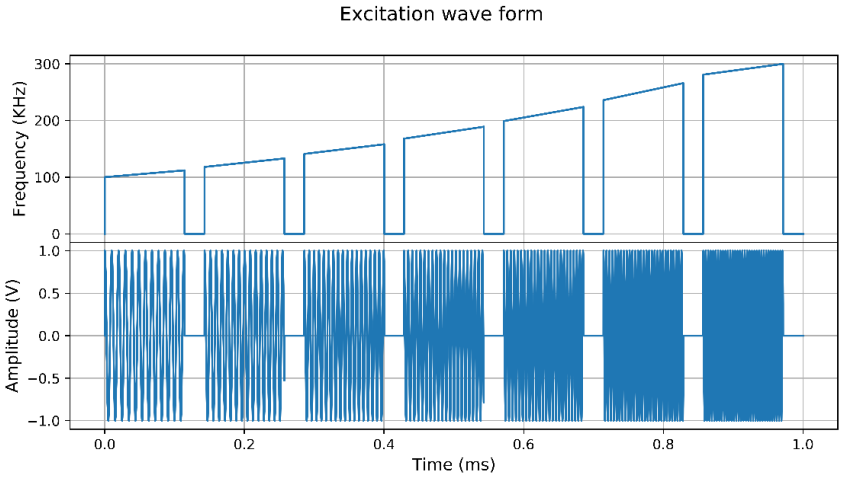

Figure 4. AU excitation signal waveform and frequency content.

2.2 Information Retrieval from Data – Signal Processing

For every anode, AU signals are collected for 18 to 21 excitation positions by the 7 receivers. Measurements were collected from rodded anodes at 18 points (instead of 21 for green, baked and sawed anodes) since they cannot be excited in positions 5, 11, and 17. Hence, a total of 126 to 147 AU signals are available for each anode. First, the continuous wavelet transform (CWT) is applied to each signal. CWT is a technique that decomposes signals into multiple frequency bands without losing time information [39]. In other words, one can, extract information that is in the time series specific to a certain frequency for detecting changes in the internal structure of the anodes. Every signal was decomposed in 7 bands: 100-112 KHz, 118-133 KHz, 141-158 KHz, 168-189 KHz, 199-224KHz, 236-266 KHz, 281-300 KHz. An example of the resulting decomposition is shown in Figure 5. With that, 7 sub-signals (time series) are obtained from every raw AU signal.

The features consist of statistics calculated from the sub-signals carrying information about the attenuated wave characteristics, and represent a unique signature of the tested carbon material. The features used in this work were: maximum value (Max), root mean square (RMS), arrival time (AT), arrival time to the maximum value (AT_{max}), signal end time (ET), the ratio between the Max and the RMS (MAX/RMS), time between features (BSep). The BSep variables are only calculated between sequential pairs of frequency bands after the lowest frequency band. The features are defined below with x(i) being the raw signal with i=1,2…I:

$$\boldsymbol{Max(x(i)) = Maximum\big(abs(x(i))\big)} \tag{1}$$

$$\boldsymbol{RMS(x(i)) = \sqrt{\frac{\sum_{i=1}^{I} x(i)^2}{N}}} \tag{2}$$

$$\boldsymbol{AT(x(i)) = i\ when\ x(i) \geq 0.3\ \cdot Max(x(i)))} \tag{3}$$

$$\boldsymbol{AT_{max}(x(i)) = i\ when\ x(i) = Max(x(i))} \tag{4}$$

$$\boldsymbol{ET(x(i)) = i\ when\ x(I-i) \geq 0.3 \cdot Max(x(i))} \tag{5}$$

$$\boldsymbol{BSep_{ET-AT}(x_1(i), x_2(i)) = AT(x_2(i)) - ET(x_1(i))} \quad (6)$$

$$\boldsymbol{BSep_{AT-AT}(x_1(i), x_2(i)) = AT(x_2(i)) - AT(x_1(i))} \quad (7)$$

$$\boldsymbol{BSep_{Max}(x_1(i), x_2(i)) = Max(x_2(i)) - Max(x_1(i))} \quad (8)$$

$$\boldsymbol{Max/RMS(x(i)) = Max(x(i))/RMS(x(i))} \quad (9)$$

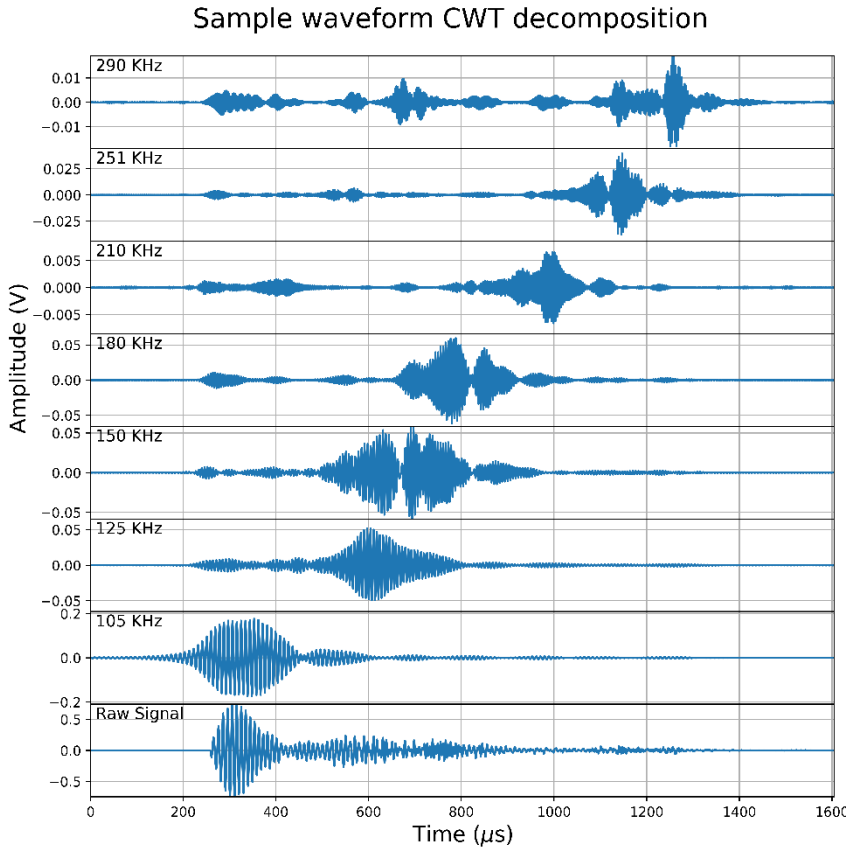

Figure 5. Example of CWT applied to the excitation waveform.

The resulting data is organized into a matrix **X** of size (N×K) prior to PCA analysis. For a given anode, the features calculated from the sub-signals at each frequency and for each excitation point are concatenated into a row vector of size (1×K), K = number of features × number of frequency bands × number of excitation points × number of receivers. The row vector obtained for each anode including repetitions are stored row-wise in **X**, where N = number of anodes × number of repeated measurements on each of them. With 12 anodes being analyzed 5 times each, the dimensions of matrix **X** are 60 × 10143 (21 excitation points x 7 receivers x (8 x(bands + raw signal) x 6 features + 7 bands x 3 features))). For rodded anodes, data referring to emitter positions 5, 11, 17 corresponding to stub hole positions are left missing.

A PCA model is built on this database. Missing data are handled by PCA when the model parameters are estimated using the Nonlinear Iterative Partial Least Squares (NIPALS). PCA reduces the dimensionality of the dataset by transforming the original features space to a new one where each dimension, denominated principal component (PC), is pointing to the direction of largest variance on the original feature space and is orthogonal to all others. The expression that defines the PCA model is:

$$\mathbf{X} = \mathbf{TP}' + \mathbf{E} \quad (10)$$

Where the **X** matrix refers to the original data, **T** is the PCA scores matrix, **P** is the loadings matrix, and **E** is the residual information. The PCA scores are the magnitude value in each of the new dimensions extracted and existing in **P**. **P** is the matrix that transforms the data between the original and transformed spaces. The dimensions in **T** and **P** are defined by the number of samples, number of original dimensions and the number of principal components used, which are typically decided by observing the variance that is accounted for using the model combined with a cross-validation routine. A subset of the full dataset is taken out of the original database, the model is built on the remaining data and then tested on the unused subset. The last matrix **E** refers to the residual information that was not captured by the model. For more details on PCA, the reader is referred to [40].

Finally, because the final space generated by the model will still be more than two-dimensional, visual inspection becomes difficult. To evaluate the capacity of differentiating anodes one by one and between different production stages, a multivariate gaussian classifier is used. Commonly referred as a Linear Discriminant, this algorithm fits a multivariate gaussian distribution for every class and assigns a class to a sample based on the estimated probabilities of this sample to be part of one of the distributions [41]. The special case of the Linear Discriminant assumes that all distributions share the same covariance matrix, which forces the separation regions to be hyper lines. This is the equivalent to separating sets of data by drawing a line between different groups in a two-dimensional chart, but in a higher dimensional space. When comparing the individual anodes, the classes represent the anode identification (id) number. When evaluating the capacity of discriminating the anodes based on production stage, the classes refers to green, baked, sawed, or rodded.

The whole signal processing is summarized in Figure 6 below:

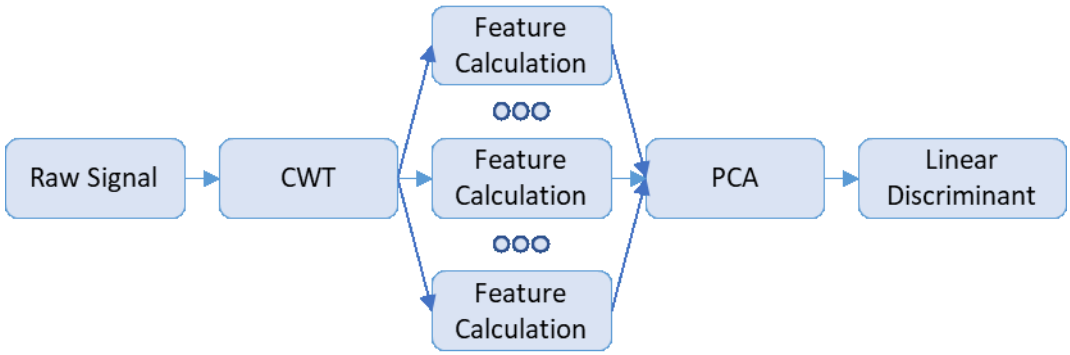

Figure 6. Signal processing block diagram.

Matlab R2018b's CWT algorithm using the "bump" wavelet was used. For the calculation of features and estimation of the PCA model, a custom python routine was built., The Linear Discriminant algorithm used was the one available in python scikit-learn library [42].

The final objective is to assess whether it is possible to discriminate the anodes AU data using hyper lines. The criterion used to evaluate that capacity is the classification score, which is simply the fraction of correct classifications. These were calculated both for the whole dataset (R^2) and through a cross-validation process. This value is calculated by dividing the dataset into subgroups, and then, for each subgroup, the model is built with all the data outside that subgroup and then the score is calculated for that group that was not used for model building. The final cross-validation score (Q^2) is the average for all the subgroups and the more subdivisions one uses, the

more trust one can give to the Q^2. The maximum subdivision number that one can use without unbalancing the dataset is 5 for the anode id, and 15 for the anode stage classifications. The matter of assessing if the repeatability is judged by observing the standard deviation of the principal components and through the Silhouette value [43]:

$$s(j) = \frac{b(j) - a(j)}{max(a(j), b(j))} \tag{11}$$

Where b(j) is the mean distance of the sample "j" to the closest different cluster of data, while a(j) is the mean distance to all of the samples inside the same cluster. The criterion ranges from -1 to 1 where a low value means that the sample "j" is closer to another cluster than it is to its own, and 1 means that the value is much closer to its own cluster than it is to other clusters.

3. Results

The resulting PCA score values for the two first principal components are plotted in Figure 7 with coloring for the anode production stage and in Figure 8 with different coloring for anode id.

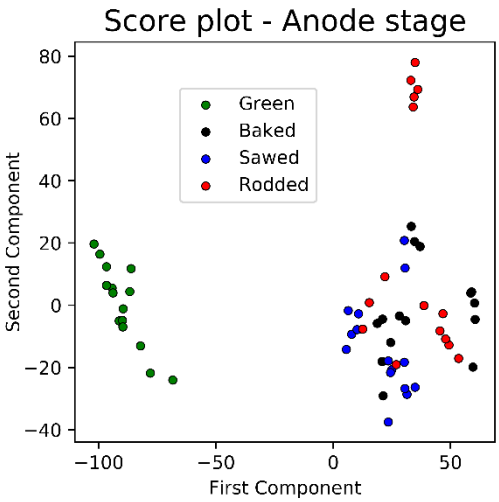

Figure 7. Anodes' 2 first principal components plotted with colors for each production stage.

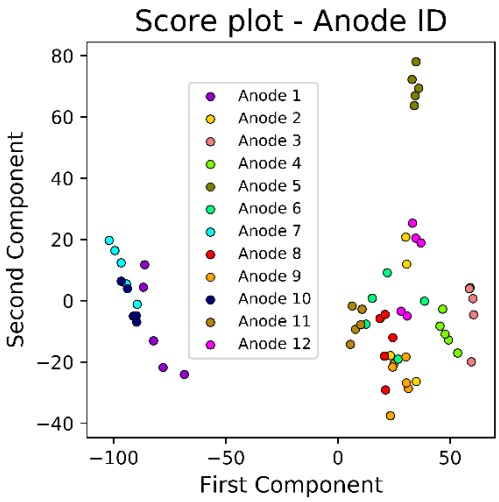

Figure 8. Anodes' 2 first principal components plotted with colors for each anode id.

By observing the two first PCs it is easy to see that green anodes separate from the others. Any anode stage other than green seems to be in the same region in the positive side of the first component. The observations with coloring for anode id numbers do not seem to show much of a trend other than anode 5 being completely separated from all other clusters. Even though there is a large mixing, each repetition of the same anode id is not so far apart on the first component, but on the second that variation is a bit more evident. An overall comparison of how much is the standard deviation in relation to the overall range for every PC is shown in Table 1.

The mean standard deviation found for each tested anode is rather high and tends to increase with the position of the principal component. The best ratio is the one on the first component, which is the equivalent to 2% of all the range found, while the worst is on the thirteenth component, with approximately 19% of all the range spanned by the experimental data collected.

Table 1. Ratio between average standard deviation for each anode and the measurement range.

PC	Std / range	PC	Std / range	PC	Std / range	PC	Std / range	PC	Std / range
1	0.02	5	0.09	9	0.10	13	0.19	17	0.17
2	0.09	6	0.09	10	0.10	14	0.17	18	0.17
3	0.09	7	0.11	11	0.16	15	0.15	19	0.16
4	0.07	8	0.10	12	0.17	16	0.16	20	0.11

The other criterion used to understand the repeatability of the measurements results is the silhouette value, which is available on Figure 9Figure below.

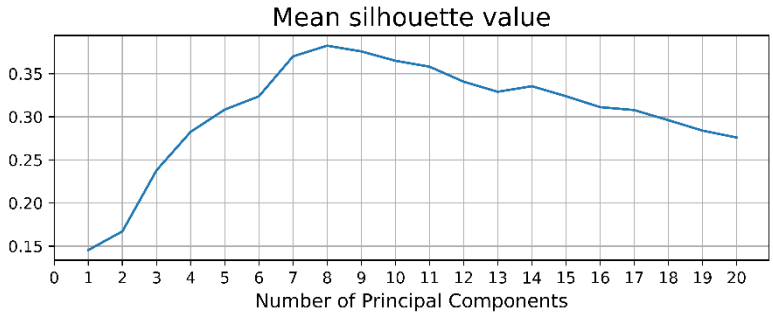

Figure 9. Mean silhouette value for all anode ids as a function of the PC number.

The value is never negative, which a sign of the clusters being separable. It peaks at 8 PCs with a value of approximately 0.37, meaning that clusters are clearly separated between themselves. That same performance is observed on the classification scores in Figure 10 and Figure 11.

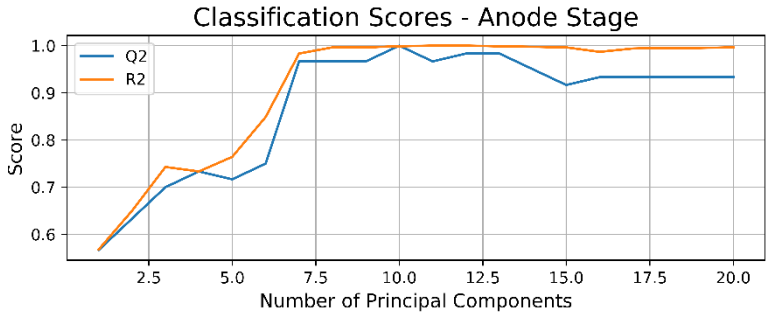

Figure 10. Linear discriminant classification score for anode stage.

The classification scores have a significantly higher value than what is achieved randomly since the first PC (0.25 on the stage classification and 0.08 on the anode id case). The cross-validation score (Q^2) is not too far below the training score (R^2). In the case of id classification, the Q^2 never touches 100% success, but the stage classification does when 10 PCs are used.

4. Discussion

The differentiation between the green anodes and all the others is very clear (Figure 7), and it seems that the first PC is just an indirect measurement of the anode's density. Such a result is not unexpected and, in fact, only supports the argumentation that a PCA applied to that data will indeed find relevant information. For the second dimension, however, the interpretation becomes more difficult, and the separation between each anode id is not evident (Figure). It even seems like the method is not precise enough to contribute with useful information. When reading Table

1, the high values of std/range ratios do suggest that the evaluation is not very repeatable, with only a 10/1 signal-to-noise ratio in most of the PCs. However, evaluating only the signal-to-noise ratios for each dimension separately is not optimal, for the model is built to be used with all of its useful PCs together. Moreover, only five measurements in each anode were executed, which may cause the standard deviation to be overestimated.

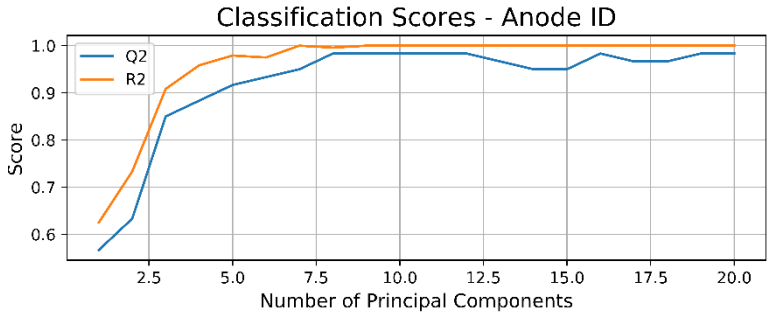

Figure 11. Linear discriminant classification score for anode id.

The repeatability of the technique only becomes evident when multiple PCs are used together, and this can be clearly observed in the Silhouette (Figure 8). A positive value such as the one found with 8 PCs allows inference that there is very little to no intersection between the clusters defined by each anode id, something that is quite remarkable given that the samples were produced in similar conditions, with similar recipes. The small to non-existent intersection is confirmed when the classification scores are observed. With 10 PCs the cross-validation (CV) score found was 1, meaning the at every single subgroup of the CV routine, the linear discriminant was capable of drawing lines that separated the anodes by production stages with a 100% accuracy (Figure 9). Such a performance is highly improbable if the system is not in fact extracting useful information from the highly dimensional dataset.

Moreover, even though classification using the anode's ids (Figure 10) could not achieve Q^2 values of 1, finding high values such as these ones is still very significant. This result is probably higher than it would be with a larger dataset not as a consequence of the technique's capacity not being enough, but because there will be anodes that are very similar just for the reason that they are being controlled to be so. It is expected that in the future, we would not be capable of separating anodes per id number as if observing their individual signatures because their signatures would be extremely similar, but the fact that we can do this in a smaller dataset points towards the method's capacity of evaluating the anodes' internal structure with depth.

5. Conclusions

Overall, the system developed achieves the objectives for which it was built. A full analysis of one anode takes an average of 40 minutes, which allows for a larger number of anodes to be analyzed in future surveys. Automating the measurement procedure would significantly reduce cycle time. The analyses are repeatable to a certain extent, but the system could extract data that allows to differentiate the green from baked anodes very clearly while still being able to separate quite well the baked anode types between themselves, even though these are not so structurally different. If one is to classify the anodes by an individual signature, the system also seems capable. All of these successful results suggest that the system is capable of extracting meaningful information about the anodes' internal structure which raises the possibility of using the system's data as a predictor of the anode's performance in the electrolytic cell, or of the risk of causing an incident during its operation. Additionally, it could also be used as a measurement for the anode

plant to control its process in a much faster response time. For any of those, full automation of the system will be required.

6. References

1. Halvor Kvande and Per Arne Drabløs, The Aluminum Smelting Process and Innovative Alternative Technologies, *J. Occup. Environ. Med.*, May 2014, vol. 56, S23–S32.
2. Meenu Gautam et al., Carbon Footprint of Aluminum Production, *Environmental Carbon Footprints*, Elsevier, 2018, 197–228.
3. Jean-Claude Fischer, The Impact of Anode Quality on Smelter Performance, Sep. 12, 2012.
4. J. A. Brown and P. J. Rhedey, Characterization of Prebaked Anode Carbon By Mechanical and Thermal Properties, *TMS Light Metals 1975*, New York, 1975.
5. Kirstine Louise Hulse, *Anode manufacture: raw materials, formulation and processing parameters*. Switzerland: R & D Carbon Ltd., 2000.
6. Ronald Barclay, Anode Fabrication, Properties & Performance, Nov. 2001.
7. Ulrich Mannweiler and Felix Keller, The design of a new anode technology for the aluminum industry, *JOM*, Feb. 1994, vol. 46, no. 2, 15–21.
8. W. K. Fischer and R. Perruchoud, Determining Prebaked Anode Properties for Aluminum Production, *JOM*, Nov. 1987, vol. 39, no. 11, 43–45.
9. Felix Keller et al., Anode Baking: The Underestimated Human Aspect, *Essential Readings in Light Metals: Volume 4 Electrode Technology for Aluminum Production*, A. Tomsett and J. Johnson, Eds. Cham: Springer International Publishing, 2016, 403–407.
10. André Charette et al., *Le carbone dans l'industrie de l'aluminium*. Chicoutimi (Québec): Les presses de l'aluminium, 2012.
11. Les Edwards et al., Evolution of Anode Grade Coke Quality, *Light Metals 2012*, C. E. Suarez, Ed. Cham: Springer International Publishing, 2012, 1207–1212.
12. Les Edwards, The History and Future Challenges of Calcined Petroleum Coke Production and Use in Aluminum Smelting, *JOM*, Feb. 2015, vol. 67, no. 2, 308–321.
13. Karl D. Bartholomew, Changes in Global Refining and Its Impact on Anode Quality Petroleum Coke, *Light Metals 2013*, B. A. Sadler, Ed. Cham: Springer International Publishing, 2016, 15–20.
14. E. A. Yanko et al., Monitoring the quality of baked anode blocks for electrolytic aluminum smelters, *Metallurgist*, Nov. 2008, vol. 52, no. 11–12, 668–671.
15. E. J. Seger, Method and means for measuring electrode resistance, US 3735253, 1974.
16. Seger, E.J., New method of measuring electric resistance for quality control, *Light Metals*, 1975.
17. M. J. Chollier-Brym et al., New Method for Representative Measurement of Anode Electrical Resistance, *Light Metals 2012*, C. E. Suarez, Ed. Cham: Springer International Publishing, 2012, 1299–1302.
18. Guillaume Léonard et al., Anode Electrical Resistance Measurements: Learning And Industrial On-Line Measurement Equipment Development, *Light Metals 2014*, J. Grandfield, Ed. Cham: Springer International Publishing, 2014, 1269–1274.
19. Guillaume Léonard et al., MIREA – An on-line real time solution to check the electrical quality of anodes, *Proceedings of 33st International Conference of ICSOBA*, Dubai, UAE, 29 November – 1 December 2015.
20. Marc Gagnon et al., MIREA: An On-Line Quality Control Equipment Integration in an Operational Context, *Light Metals 2016*, E. Williams, Ed. Hoboken, NJ, USA: John Wiley & Sons, Inc., 2016, 977–984.
21. Duygu Kocaefe et al., Method for analyzing an anode and device thereof, US 10281421 B2, May 07, 2019.
22. D. Kocaefe et al., Measurement of anode electrical resistivity for quality control in aluminium industry, *53rd COM*, Vancouver, British Columbia, Oct. 2014.

23. Marc-Alain Andoh et al., Measurement of the Electric Current Distribution in an Anode, *Light Metals 2016*, E. Williams, Ed. Cham: Springer International Publishing, 2016, 889–894.
24. Yasar Kocaefe et al., Quality Control via Electrical Resistivity Measurement of Industrial Anodes, *Light Metals 2015*, M. Hyland, Ed. Cham: Springer International Publishing, 2015, 1097–1102.
25. Abderrahmane Benzaoui et al., A Non-Destructive Technique for the On-Line Quality Control of Green and Baked Anodes, *Proceedings of 34st International Conference of ICSOBA*, Québec, Canada, 2016.
26. Abderrahmane Benzaoui et al., A Non-Destructive Technique for the On-Line Quality Control of Green and Baked Anodes, *Metals*, 2017, vol. 7, no. 4, 128.
27. Abderrahmane Benzaoui et al., An experimental testing of the SERMA technology for the quality control of green and baked anodes, *Proceedings of 35st International Conference of ICSOBA*, Hamburg, Germany, Oct. 2017.
28. Yasar Kocaefe et al., Testing of SERMA Technology on Industrial Anodes for Quality Control for Aluminum Production, *Light Metals 2020*, Cham, 2020, 1189–1195.
29. Donald P. Ziegler and John Secasan, Methods for Determining Green Electrode Electrical Resistivity and Methods for Making Electrodes, US 9416458 B2.
30. L. J. Van der Pauw, A Method of Measuring Specific Resistivity and Hall Effect of Discs of Arbitrary Shape, *Semiconductor Devices: Pioneering Papers*, World Scientific, 1991, 174–182.
31. Adéline Paris et al., Development of a Soft Sensor for Detecting Overpitched Green Anodes, in *Light Metals 2020*, Cham, 2020, 1176–1182.
32. Paul R. Haldemann and Eman P. Fawzi, Method and Apparatus for Non-Destructively Detecting Flaws In a Carbon Anode, US 5473248 A, 1995.
33. Fawzi Emad et al., The in-line inspection of carbon anodes for aluminum production, *JOM*, Feb. 1996, vol. 48, no. 2, 24–27.
34. Daniel Audet and Luc Parent, System and Method to Forecast the Electrical Conductivity of Anodes for Aluminum Production Before Baking, US 7576534 B2, 2004.
35. Weng Tu-Lung, Quality Evaluation of Carbonaceous Materials by Ultrasonic Techniques, *Light Metals*, 1981.
36. Moez Ben Boubaker et al., The Potential of Acousto-Ultrasonic Techniques for Inspection of Baked Carbon Anodes, *Metals*, Jul. 2016, vol. 6, no. 7, 151.
37. Moez Ben Boubaker et al., Inspection of Prebaked Carbon Anodes Using Multi-Spectral Acousto-Ultrasonic Excitation, *Metals*, Aug. 2017, vol. 7, no. 8, 305.
38. Moez Ben Boubaker et al., Inspection of baked carbon anodes using a combination of multi-spectral acousto-ultrasonic techniques and principal component analysis, *Ultrasonics*, Sep. 2018, vol. 89, 126–136.
39. S. G. Mallat, A theory for multiresolution signal decomposition: the wavelet representation, *IEEE Trans. Pattern Anal. Machine Intell.*, Jul. 1989, vol. 11, no. 7, 674–693.
40. Svante Wold et al., Principal Component Analysis, *Chemom. Intell. Lab. Syst.*, 1987, 37–52.
41. Seymour Geisser, Posterior Odds for Multivariate Normal Classifications, *Journal of the Royal Statistical Society. Series B (Methodological)*, 1964, vol. 26, no. 1, 69–76.
42. Fabian Pedregosa et al., Scikit-learn: Machine Learning in Python, *Journal of Machine Learning Research*, 2011, vol. 12, no. 85, 2825–2830.
43. Peter J. Rousseeuw, Silhouettes: A graphical aid to the interpretation and validation of cluster analysis, *Journal of Computational and Applied Mathematics*, Nov. 1987, vol. 20, 53–65.